

Chapter 1

Understanding and Applying Single Tip Plasmonics

As discussed in the theoretical background (chapter ??) only a small amount of work has been done to characterise and understand tips prior to applying them as optical nanoantennae. Understanding this interaction between tips and far-field light has been one of the main motivations of this project. A hyperspectral imaging technique is applied to laterally map light scattering from a tip with confocally localised spectra to infer a local optical response and better study different tips. Understanding this response at the apex of single tips is of importance in determining their effectiveness as near-field enhancers and in understanding their coupling behaviour in the presence of another tip. In this chapter the spectra of single tips is discussed, studying both sharp and spherical-tipped Au AFM probes, along with the application of spherical Au tips to Raman spectroscopy.

1.1 Optical Characterisation of Nanostructures using Hyperspectral Imaging

Hyperspectral imaging encompasses a range of optical techniques which image using pixels comprised of a spectrum rather than an RGB colour value. This is advantageous over regular imaging as more quantitative information can be extracted from an image. Hence hyperspectral imaging techniques have become commonplace across many diverse fields, including microscopy [1, 2], astrophysics [3], remote sensing and geology [4, 5], food standards [6, 7], and medical imaging [8–10]. Within each of these fields, the features in an image are more clearly identified by their spectral signatures. In this instance, scanning confocal hyperspectral imaging is applied to optically characterise both sharp and nanostructured metallic tips and identify surface plasmon resonances (SPRs) originating from localised surface plasmon (LSP) excitation.¹

¹This technique has also been applied to other periodic, extended nanostructures that are not discussed within the context of this thesis.

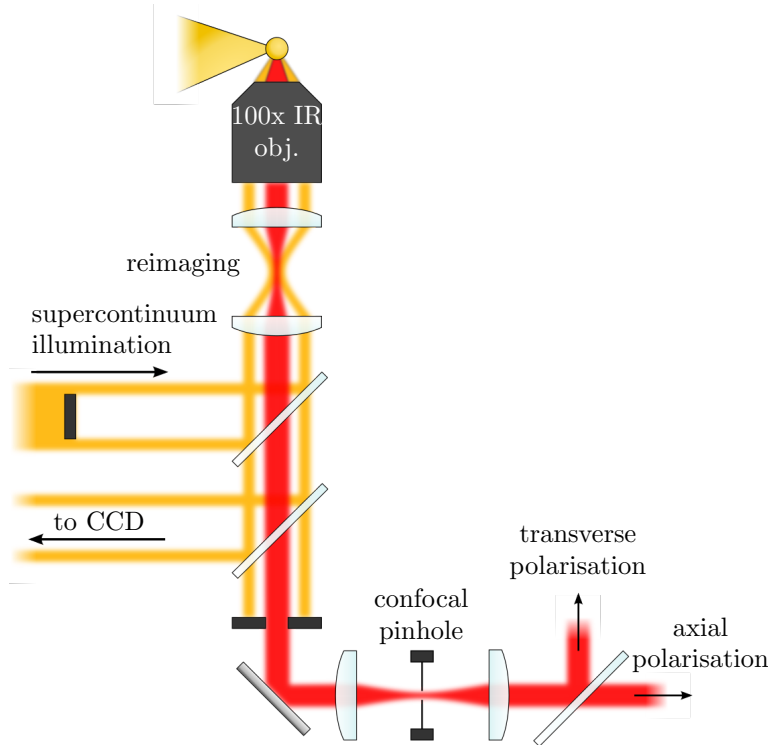


Figure 1.1: Experiment configuration for hyperspectral imaging. The laser is centered on the tip apex for imaging. The tip is scanned across the beam in a grid with spectra acquired at each position. The resulting image then contains 1044 colours at each pixel instead of the usual 3 (RGB).

Scanning confocal hyperspectral imaging falls under the category of spatially scanned imaging. Tips are scanned in a grid under the laser spot and the spectral content of the confocal sampling volume is measured at each point using a spectrometer instead of a photodiode or CCD. Images are then formed at a given wavelength or across a wavelength band. In this instance, using a spectrometer, each image pixel is digitised into 1044 bins between 400–1200 nm rather than the conventional 3 RGB colour bands. The 0.8 nm wavelength resolution of spectra classifies this procedure as hyperspectral, as opposed to multi-spectral imaging in which images are formed using fewer, much broader, wavelength bands. This approach to hyperspectral imaging has previously been used to identify distributed plasmon modes in aggregated AuNP colloids [11] and to image SPPs [12]. By using this technique in the current microscope configuration, as shown in Figure 1.1, LSPs can be spatially identified with sub-diffraction-limited resolutions around 250–300 nm. Combining it with 80 nm AuNPs also enabled measurement of the microscope PSF and chromatic aberrations, as discussed in chapter ??.

Fast image acquisition is made possible by utilising the ultra-high brightness supercontinuum laser source and sensitive, TE-cooled, bench-top spectrometers with 10–20 ms integration times. Image acquisition is limited only by the integration time at each pixel and the ~30 ms movement time between pixels. The focal intensity is, on average, $\sim 10^5 \text{ W cm}^{-2}$, which is below the damage threshold for 50 nm metallic tip coatings. The illumination and collection

configuration is fixed using a preset reference intensity between different samples in order to more quantitatively compare images. Measured spectra of metallic nanostructures are normalised to a BF reflection spectrum of the same flat metal to show structural effects only, such as plasmons.

While not the fastest or most advanced method of acquiring hyperspectral images, spatial scanning is made efficient when used with a supercontinuum white-light source. Other imaging techniques, categorised under “spectral scanning”, “non-scanning” and “spatio-spectral scanning”, have been developed to more efficiently produce hyperspectral images under specific conditions. Spectral scanning involves wide-field imaging through either a range of bandpass filters [13], a tuneable liquid crystal filter [14, 15] or an etalon [16], which is appropriate if studying large areas or if confocal localisation is not required. Similarly, if the benefits of optical sectioning are not necessary, a single direction line scan over a sample can be performed with an imaging spectrograph (monochromator with CCD) to form a hyperspectral image rather than use a two-dimensional grid scan with single pixel acquisition [1].

Non-scanning or snapshot hyperspectral imaging techniques are more complex than scanning techniques as both spatial and spectral information are acquired in a single measurement without any scanning or dynamic filtering. The main method of achieving this is by using a computed tomography imaging spectrometer (CTIS) [17–20], in which a 2D dispersive grating placed in the Fourier plane splits an image into many separate spectral images projected onto a CCD. Advantages of this approach are much shorter acquisition times but necessitates a higher computational requirement to disentangle the 2D image into a cube with dimensions (x, y, λ) . Spatio-spectro scanning is the most recent technique, developed in 2014, and involves diagonally scanning through the sample data cube where each point along an axis in the spatial image has a different wavelength [21].

Despite the potential improvements gained by using more advanced hyperspectral imaging techniques, spatial point scanning is deemed the most appropriate solution for tip characterisation, if only for simplicity and compatibility with dual-tip gap spectroscopy. Image acquisition is not time-constrained since the microscope platform is stable, resulting in minimal artefacts due to sample motion, and the use of confocal imaging benefits image quality. Spectral scanning is not beneficial at the current magnification due to the relatively small area occupied by the sample in the wide-field image and due to the far superior spectral resolution of spectrometers when compared to imaging through bandpass filters. For these reasons, spatial point scanning is used for characterisation.

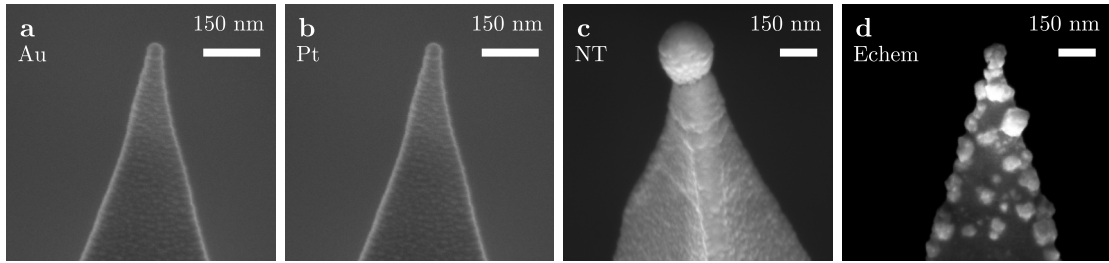


Figure 1.2: SEM images of sharp and spherical metal tips studied using hyperspectral imaging. Tips are (a) a sharp Au AFM tip, (b) a sharp Pt AFM tip, (c) a NT Au-coated spherical AFM tip and (d) an electrochemically deposited AuNP-on-Pt AFM tip.

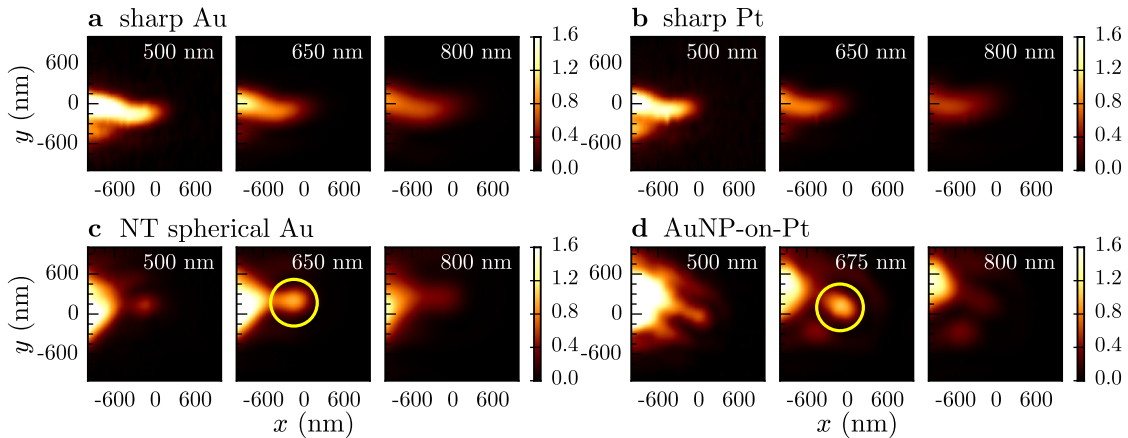


Figure 1.3: Hyperspectral images of sharp and spherical metal tips at wavelengths of interest. Images are of (a) a sharp Au tip, (b) a sharp Pt tip, (c) a NanoTools Au-coated spherical tip and (d) an electrochemically deposited AuNP-on-Pt tip. Collection polarisation is along the tip axis. Colour maps between slices all have the same normalisation. Resonant scattering from spherical apices is clearly seen in the hyperspectral images of between 600–700 nm and highlighted by yellow circles.

1.2 Understanding Plasmons in Spherical Nanoparticle Tips

Hyperspectral images are taken of four different types of AFM probes to investigate the plasmonics of nanostuctured tips. AFM tips studied are Au- and Pt-coated standard AFM probes (BudgetSensors Au-coated AFM probes), spherical Au tips (300 nm Au-coated NanoTools B150 AFM probes) [22] and AuNP-on-Pt AFM probes, fabricated in-house using electrochemical deposition [23]. SEM images of a selection of these tips are shown in Figure 1.2. Fabricated tips are pre-treated where possible prior to use with piranha solution to remove organic surface residue and, in some cases, smooth surface roughness.

Comparisons between spherical- and sharp-tipped metallic probes using hyperspectral image slices (Figure 1.3) show that spherical Au tips exhibit a characteristic red (600–700 nm) scatter, delocalised from the bulk tip. No similar localised scattering is seen for sharp Au or Pt

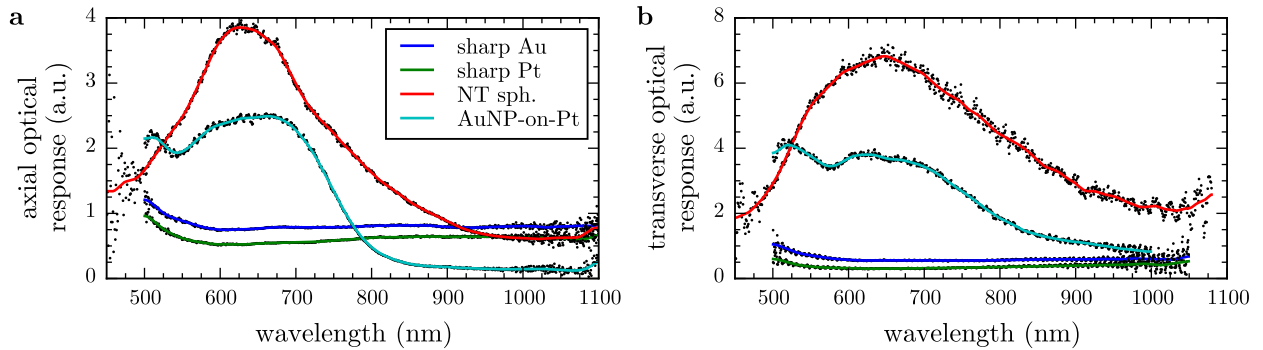


Figure 1.4: Apex spectra of sharp and spherical metal tips. Spectra are extracted from the hyperspectral images in Fig. 1.3 by integrating pixels around the apex region. A clear resonance at 630 nm is observed with spherical tips in both polarisations. The axial/longitudinal tip resonance is blueshifted 20 nm from the longer transverse resonance. Sharp metallic tips show comparatively flat spectra.

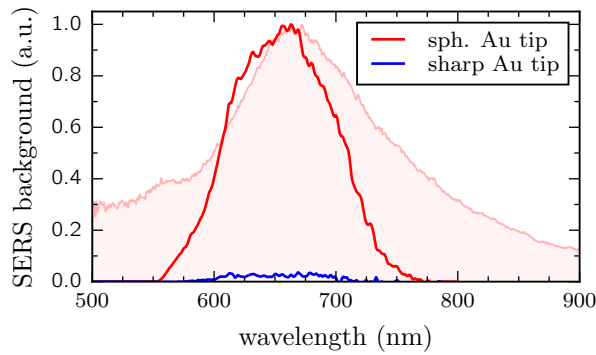


Figure 1.5: Integrated inelastic electron fluorescence measurements of both a sharp and spherical Au tip. Fluorescence spectra are acquired using tuneable, single wavelength spectroscopy with integrated spectra plotted as a function of excitation wavelength. The background spectrum is the supercontinuum dark-field scattering spectrum of the spherical Au tip apex, as measured using hyperspectral imaging. Agreement between the fluorescence (near-field) and dark-field scattering (far-field) spectra confirms resonant near-field enhancement as a LSP excitation. Sharp Au tips show no such resonance in either the near-field or far-field.

tips in the visible spectrum, which have an overall weaker optical response. This delocalised apex scatter can also be clearly seen in wide-field DF imaging. SEM images confirm that this scatter correlates only with spherical Au tip shapes, or when a AuNP is securely attached at the tip apex with a sufficiently small neck joint.

Integrating spectra around tip apices confirm that only spherical Au tips exhibit structural resonances (Figure 1.4). Scattering resonances around 630 nm are reliably present in all spherical-tipped AFM probes, both vacuum-processed and electrochemically deposited AuNP-on-Pt, and are attributed to direct LSP excitation. The response of sharp Au tips shows no similar plasmonic features while the slow rise in scattering towards the NIR is consistent with lightning rod scattering [24].

Broadband tuneable SERS [25] on each of the tips is used to confirm that the resonance

is indeed a LSP by showing that the internal near-field is resonantly enhanced.² During plasmon excitation both internal and external fields are enhanced. The external field leads to the strong enhancement of Raman spectra whereas inelastic electron scatter insider the surface of the metal is enhanced by the internal field, forming the SERS background [26]. Broadband tuneable SERS is a technique capable of showing both these components [25]. Hence, by integrating the inelastic scattering background at each wavelength the near-field resonance can be calculated.³ SERS background spectra are taken in 10 nm increments of the excitation wavelength.⁴ Integration of the scattering counts for each excitation wavelength shows a distinct peak (Figure 1.5) around the scattering resonance from Figure 1.4, confirming it as a LSP resonance. Further, confirmation stems from direct observation of plasmon coupling between spherical tips, as has been previously reported [22], with results of the latest tip coupling experiments discussed in detail in the next chapter.

Surprisingly, the overall disorder and parasitic edge AuNP nucleation on AuNP-on-Pt only minimally effects the overall optical response from the apex growth. This is likely because the spherical apex already interacts with the base tip structure, regardless of any further deposits. The AuNP-on-Pt structure behaves very similarly to the Au-coated diamond-like-carbon spherical tip, likely because the 50 nm coating thickness is greater than the skin depth [27, 28]. Plasmons therefore see both as solid Au spheres. Differences arise due to the differences in neck material with Au-Pt and Au-Au neck boundaries.

1.2.1 Interpreting the Spectral Response of Metallic Tips

The plasmon modes of a spherical Au tip are not so different from those of a spherical AuNP and can be explained accordingly. Like AuNP plasmons, spherical tip LSPs are specifically *radiative* antenna-like modes, those that can efficiently couple far-field light into strong collective free electron oscillations without the need for momentum matching due to SPP dispersion. As with AuNPs, the signature of these plasmons is a distinct SPR indicating their large dipole moment, as seen in Figures 1.4 and 1.5. Radiative antenna-like LSPs form only when two close dielectric surfaces surround a metallic particle, allowing the formation of confined multipolar charge oscillations where the geometry modifies the oscillation restoring forces and determines the resonant wavelength [29, 30]. Spherical metal tips retain some of the back hemisphere around the connection to the base tip apex (the neck), allowing the spherical apex surfaces to sustain similar antenna-like plasmons. Sharp tips do not have this back surface, hence cannot support such resonances. Their metal-dielectric surface still, however, supports the launching of SPPs in the near-field if the correct launching conditions are satisfied. This requirement

²Acquisition of broadband tuneable SERS measurements carried out by A. Lombardi.

³Model of this behaviour is derived in the appendix.

⁴Each acquired background spectrum is shown in the appendix

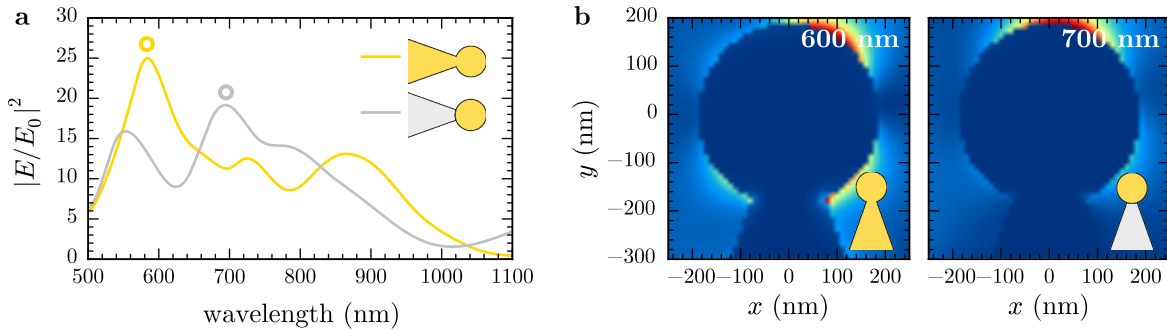


Figure 1.6: Numerical simulations of the field enhancement around a spherical Au tip.
 (a) Near-field spectra of spherical Au and AuNP-on-Pt tips, extracted from around the apex of the tip.
 (b) Near-field enhancement distributions of the two resonances highlighted by circles in (a). Simulated tips have a 300 nm spherical radii, 120 nm neck widths, 20° opening angles and 1.88 μm lengths.

means that while a sharp tip can in some ways be considered an optical antenna its supported modes are considered as *evanescent* or *near-field* modes rather than *radiative*, limiting its usability.

Numerical simulations of the near-field around spherical tips, computed using BEMAX, are used to show aspects of antenna-like behaviour and can be used to qualitatively describe tips.⁵ Simulated spectra of the near-field around the apices of 300 nm spherical Au and AuNP-on-Pt tips with 120 nm neck diameters and 20° opening angles are shown in Figure 1.6a. Tips are simulated with a length of 1.88 μm to avoid significant truncation artefacts. A neck width of $d_{\text{neck}} = 0.4d_{\text{sphere}}$ (120 nm in this case) is used to match typical experimental structures. Strong modes appear for both tips between 550–700 nm similar to experiments. The peak positions of the strongest resonance in each tip approximately agree with the experimental spectra shown in Figure 1.4a. Near-field maps corresponding to the main resonance in each tip are shown in Figure 1.6b. The near-field at the dominant resonance in the spherical Au tip appears more quadrupole-like with a weaker dipole-like resonance occurring above 700 nm. These are similar to the modes in the AuNP-on-Pt tip except redshifted with different intensities. The 700 nm resonance in the AuNP-on-Pt tip has a more dipole-like structure with a more quadrupole-like resonance at 550 nm.

Spectra can be explained by realising that quadrupolar visible modes are more favourable in larger AuNPs, as found in Mie scattering theory, once dipolar resonances shift out into the NIR. A similarly structured mode to the AuNP quadrupole plasmon would be expected in 300 nm spherical Au tips between 500–600 nm. The neck geometry can potentially short the pole of dipolar plasmons, reducing their confinement, whereas quadrupolar plasmons are much less affected, leading to a more favourable charge distribution and larger SPR. Restoring forces are very different in spherical tips than nanospheres, however, since the neck removes a

⁵BEMAX simulations carried out by D. O. Sigle.

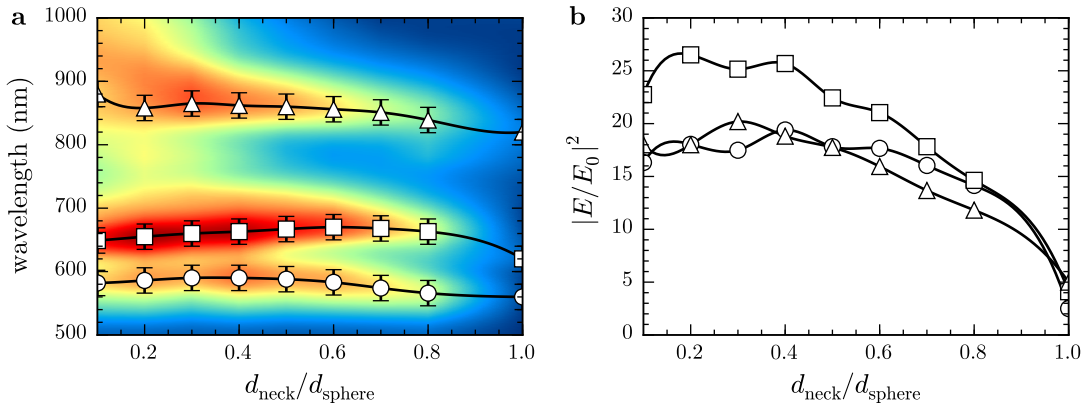


Figure 1.7: Resonant wavelength and field enhancement dependence on the neck width. The resonant wavelength (a) and field enhancement (b) for each of the resonances in spherical Au tips of 250 nm sphere diameter, 1.88 μm length, and 10° opening angle of varying neck widths.

portion of the back sphere surface and introduces conductive losses, and the tip exiting close to the rear surface provides a secondary surface for self-interaction. This makes them difficult to analytically describe.

Electromagnetic coupling between Au and Pt surfaces is weaker than the interaction between two Au surfaces [31], hence plasmons in the Au sphere are less redshifted when attached to a Pt tip apex. The non-plasmonic Pt neck region also forms an additional boundary interface to better confine plasmons to the AuNP. Hence, the redshift of AuNP-on-Pt tips is much less pronounced. The dipole-like mode exists nearer to the visible and therefore becomes more favourable than the quadrupole-like mode or becomes easier to couple to. Failure to experimentally observe the predicted quadrupole-like mode suggests that either the dipolar mode is a far more energetically favourable charge configuration or that the simulated geometry remains too dissimilar to realistic spherical tips. Nevertheless, simulations provide some insight and qualitative descriptions from which to understand plasmons in spherical metallic tips.

In order to directly compare the *plasmonic* behaviour of spherical Au tips with sharp Au tips independent of the lightning rod contribution, the neck width is increased in simulations with spectra extracted as before. In this manner, the structure transitions from a AuNP attached to the apex of a sharp tip into a more typical spherical tip followed by a transition into a rounded tip geometry, similar in shape to a sharp Au tip, without the radius of the tip apex ever changing. **A smaller radius of curvature and opening angle are used to fall between the expected behaviour of both sharp and spherical tips.** The field enhancement and peak positions extracted from the results of this morphology transition are shown in Figure 1.7. Resonances do not appear to be particularly sensitive to neck width until it becomes greater than $0.8d_{\text{sphere}}$ and the tip transitions into a geometry more similar to sharp tips. This explains the robustness of observed spherical tip plasmons regardless of tip morphology. A steady decrease in the field enhancement, however, is observed once $d_{\text{neck}} > 0.4d_{\text{sphere}}$, decreasing

faster once $d_{\text{neck}} > 0.8d_{\text{sphere}}$. This supports the claim that sharp tips lack a back surface on which to sustain antenna-like LSPs.

1.2.2 Implications of Spherical Metallic Tip Plasmonics

The previously presented results demonstrate that it is important to consider what plasmons might exist in a particular nanostructure geometry under certain illumination and collection conditions, and that it is vital to characterise nanostructures before applying them in any further techniques. Without prior knowledge as to where in the visible spectrum specific plasmons are excited it is difficult to properly interpret any further results, such as TERS spectra. Improved tip characterisation is crucial to understanding why such varied TERS enhancements are reported. Additional thought must also be given to the optical method of characterisation. Confocal hyperspectral imaging is capable of mapping the local scattering response due to use of a pinhole for localisation. Broadband tuneable SERS also offers a unique way of characterising the near-field. Basic microscopy alone is a not particularly effective method for measuring the apex response of a tip and thus techniques similar to those described in this chapter should be used and developed wherever and whenever possible.

Utilising spherical tips not only exploits visible LSPs but also permits the use of a wider range of illumination configurations as the restriction to evanescent coupling is lifted. Regardless of plasmonics, the lightning rod effect will always play a role in the near-field enhancement process, giving sharp tips an initial advantage, but with careful optimisation of the spherical tip geometry, tips can be brought into resonance with one of the plasmons to maximise enhancement. Spherical Au tips in their current form are already quite well optimised for TERS due to being on resonance with the readily available HeNe laser wavelength often used.

Plasmons in spherical tips have also been shown to readily couple with plasmons in other spherical tips [22] and would be expected to couple with image charges in a planar mirror, thus significantly increasing their near-field enhancement. In this situation, their resonances can be tracked as the tip approaches the surface and stopped on resonance with the incident TERS laser for maximum enhancement, for example at the common 785 nm excitation wavelength. For small gaps on the nanometre level, the plasmon mode will become strongly confined to the gap and its contribution to the near-field should outweigh the lightning rod effect. Exploiting the radiative plasmons in nanostructured tips in this manner bridges the gap between the plasmonics involved in SERS and TERS. Some of the largest enhancement factors recently measured in plasmonic systems originate from radiative plasmons in AuNPs coupled with the charge distribution of their image in a mirror [32, 33]. These systems repeatedly produce Raman enhancements of up to 10^7 , much like tips, with nanometric mode volumes of coupled plasmons. This demonstrates that plasmonic gaps can exhibit large field enhancement without requiring a significant contribution from the lightning rod effect. However, the static nature

of the NPoM geometry lacks the ability to chemically map a surface. By coupling plasmons in spherical tips with their mirror charge, surfaces could be dynamically mapped with a potentially very large field enhancement.

This discussion on single tip plasmonics is concluded by performing one measurement specifically relevant to TENOM. To demonstrate the advantages of having prior knowledge of excited plasmons in tips, along with the advantages of using AuNP-on-Pt tips, a TERS measurement is performed directly after characterisation on resonance with a plasmon.

1.3 Improved Field Enhancement of Spherical Au Nanoparticle Tips

A result of spherical Au tips sustaining SPRs which couple with the far-field is that their plasmonic contribution to the field enhancement can outperform the lightning rod contribution in sharp tips (assuming no near-field plasmonic excitation in sharp tips). The field enhancements for both sharp and spherical Au tips, more specifically the fabricated AuNP-on-Pt tips, are determined in a side illumination configuration by using Raman scattering.

SDF spectroscopy is used in conjunction with Raman spectroscopy in a modified version of the microscope platform, enabling both techniques (though not simultaneously). Fabricated AuNP AFM tips are mounted opposite a benzenethiol-coated sharp Au AFM tip in a tip-to-tip configuration, mimicking a plasmonic bow-tie antenna (Figure 1.8). This configuration is used to obtain good optical access to the intertip gap for spectroscopically probing its plasmonic properties. Benzenethiol (BTh) is used as a Raman marker for measuring the relative field

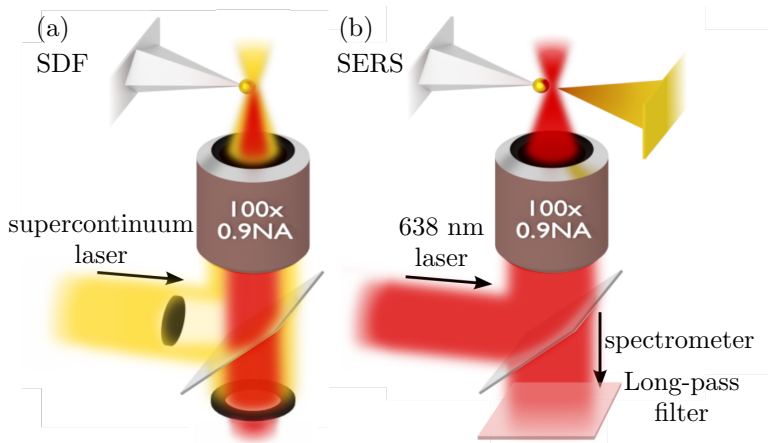


Figure 1.8: Experimental geometry for dark-field spectroscopy and SERS measurements. A 125 nm radius spherical AuNP grown onto a Pt-coated AFM tip is spectroscopically studied using a supercontinuum laser in a dark-field configuration (a). The tip is then brought within 1 nm of a benzenethiol-coated sharp Au tip under 638 nm illumination to measure SERS spectra (b).

enhancement of AuNP tips due to its strong Raman response and well-known spectra [34, 35]. BTh (VWR International Thiophenol for synthesis) is diluted to 5 mM solutions in ethanol (Sigma-Aldrich). A standard Au-coated AFM tip, for use as a SERS substrate, is prepared by coating a monolayer of BTh onto the surface. This is achieved by submerging it in 100 mM ethanolic BTh solution for 1 min followed by rinsing with ethanol and drying in nitrogen. This is repeated 5 times to ensure complete monolayer coverage. Tips used as plasmonic probes are not coated in BTh.

With the BTh tip retracted, a SDF apex scattering spectrum of the enhancing tip is acquired. After characterisation the microscope optics are modified into a TERS configuration and the enhancing tip is aligned to the BTh tip using the capacitive alignment technique described in chapter ??.⁶ Once aligned, the gap size is reduced to ~ 1 nm, limited by the thickness of the assembled BTh molecular layer, and illuminated through a 100×0.9 NA visible objective with 3 mW (1.9 MW cm^{-2}) of 638 nm laser light incident on the gap, polarised along the tip axis. Scattered light is collected through the same objective and confocally localised. Raman spectra are filtered using a 650 nm long-pass filter (Chroma) prior to dispersion in a spectrometer. Contact dynamics, measured using AFM, confirm that tips come into physical contact while separated by a BTh layer.

Near-field calculations for the spherical Au tip are computed for comparison with experimental results and to understand the enhancement mechanism. The near-field distribution at 633 nm and the spectrum 1 nm from the apex are calculated using the full electrodynamic boundary-element method [36, 37].⁷ The spherical tip is modelled as a Pt cone with half-angle 20° with a 250 nm diameter AuNP attached to its end. The neck diameter between sphere and tip is 100 nm. The tip is illuminated with a plane wave polarised along the tip axis.

A 250 nm diameter spherical AuNP-on-Pt tip, grown as described in chapter ?? (-8 V, 150 ms exposure), is used to demonstrate the augmented plasmonic properties of spherically nanostructured tips. Raman spectra of BTh molecules in the tip dimer gap are greatly enhanced when using a AuNP tip in place of a sharp Au tip (Figure 1.9a). As the same spectrometer is used for both broadband scattering spectra and SERS spectra, its restricted spectral resolution (300–1100 nm bandwidth), combined with the broadness of the diode laser line illumination, blurs the characteristic multiple Raman peaks of BTh between $1000\text{--}1600 \text{ cm}^{-1}$. However the resulting observation of two broad peaks in this region affirms the presence of BTh in the gap between tips. **Absence of a S-H peak around 2200 cm^{-1} suggests good monolayer coverage.** The background signal is also enhanced across a broad bandwidth, as is typical for SERS [34].

Supercontinuum dark-field (SDF) scattering spectra (Figure 1.9b), taken of individual tips prior to SERS measurements, show that the increased Raman enhancement when using a

⁶The optics are modified in the sense that the laser input is switched and the dark-field iris is opened.

⁷Near-field calculations carried out by Lars O. Herrmann.

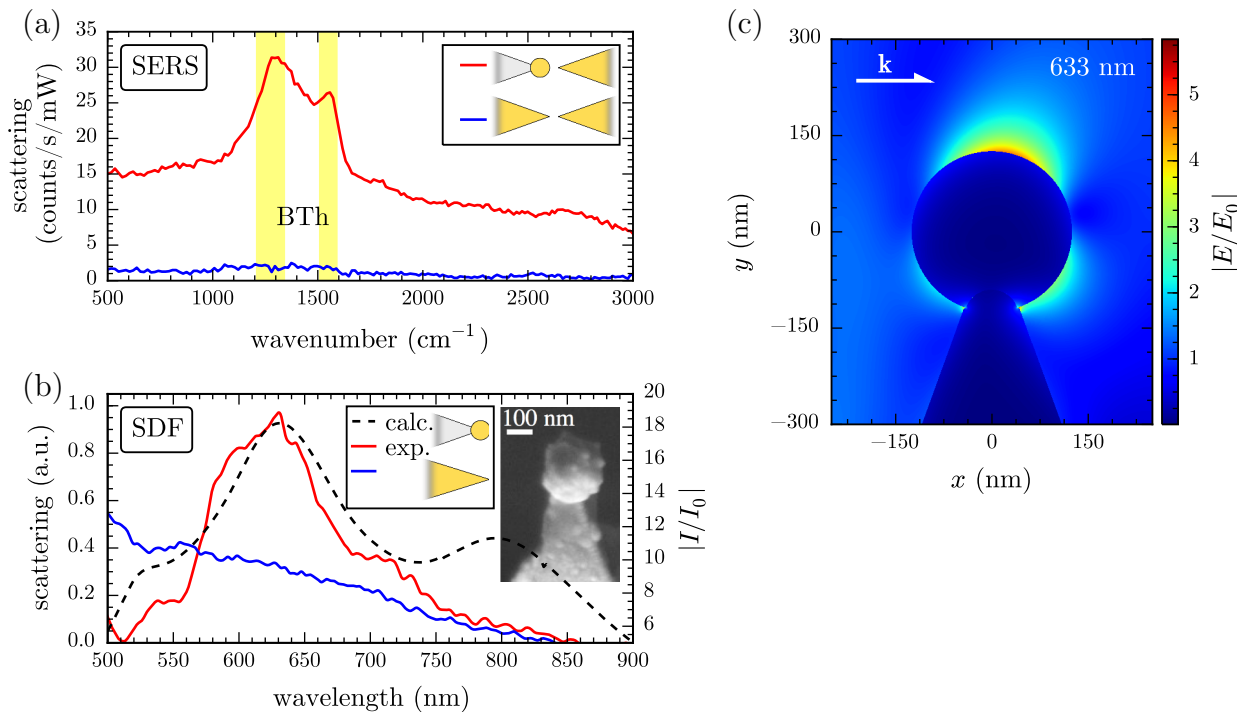


Figure 1.9: Application of sharp Au and AuNP-on-Pt tips to enhancing Raman scattering. (a,b) Comparative TERS and dark-field spectroscopy of sharp Au and AuNP tips. (a) Tip-enhanced Raman spectra of a benzenethiol-coated Au AFM probe brought close to the AuNP tip (red), compared to a sharp Au AFM tip (blue). (b) Dark-field optical scattering of AuNP (red) and sharp Au (blue) AFM tips, with calculated relative intensity enhancement 0.5 nm from the AuNP tip apex (dashed). The inset shows an SEM image of the 250 nm AuNP tip. (c) Calculated field enhancement profile for a 250 nm diameter AuNP at the end of a 1500 nm long Pt tip. The neck join is 50 nm wide and the tip is under longitudinally polarised plane wave illumination at 633 nm.

AuNP tip is due to excitation of a LSP around 630 nm, not present in sharp Au tips. This is in good agreement with boundary element calculations of the near-field enhancement at the AuNP tip apex with a visible plasmon resonance observed across the AuNP (Figure 1.9b,c). Coupling between this LSP in the AuNP tip with a BTh-coated sharp Au tip forms a confined gap plasmon mode. Since coupling is between higher order modes in the sharp Au tip, shifting of this resonance as a function of gap size is weak [38, 39]. Illuminating on resonance with the AuNP tip plasmon therefore greatly increases the Raman response by 30× when compared with the sharp Au tip Raman response. A relative SERS enhancement is estimated by taking into account the confinement and mode volume of a LSP in the gap in each case.

LSP mode volumes are estimated using a cylindrical gap mode model. The lateral width of a gap plasmon mode is calculated using $w = \sqrt{R_{\text{eff}}d}$, where R_{eff} is the effective radius of the particles, $\sqrt{R_1 R_2}$, comprising the plasmonic dimer and d is the width of the gap separating particles [40].⁸ This results in lateral mode widths of 4.5 nm for the sharp Au tip of 20 nm

⁸The use of $R_{\text{eff}} = \sqrt{R_1 R_2}$ is justified by...

radius and 7.1 nm for the 125 nm radius AuNP tip.⁹ Assuming a cylindrical gap mode yields mode volumes of 15.7 nm³ and 39.3 nm³, respectively. These define the near-field contribution to Raman scattering and a relative field enhancement is obtained using,

$$FE_{\text{rel}} = \frac{N_{\text{AuNP}}/V_{\text{AuNP}}}{N_{\text{tip}}/V_{\text{tip}}} \quad (1.1)$$

where N is the Raman signal counts and V is the mode volume. This evaluates to a relative SERS enhancement of 12. Since the LSP is laterally confined to only 7 nm within this gap the enhanced Raman signal is the result of scattering contributions from only a very small number of molecules. Lower limit absolute Raman enhancements are estimated using,

$$FE_{\text{abs}} = \frac{N_{nf}/V_{nf}}{N_{ff}/V_{ff}} \quad (1.2)$$

where N_{ff} , the number of counts obtained using only far-field laser light, is assumed to be 0.1 counts/s/mW from the noise levels since signals are below the signal to noise level and V_{ff} is assumed to be 25 000 nm³ based upon the surface of a conical tip exposed to the focal volume of a diffraction limited spot ($d = 412$ nm at $\lambda = 638$ nm). This expression yields absolute, lower-bound Raman enhancements of 1.9×10^5 for a 250 nm AuNP tip and 1.6×10^4 for a sharp Au tip. Though absolute estimates are not as high as the expected 10^7 – 10^8 enhancements reported in the literature [41], the relative SERS enhancement observed with the AuNP tip is indeed comparable to previously reported results [42].

These optical measurements confirm that AuNP tips provide increased field enhancement compared to sharp Au tips due to a strong LSP excitation. Lack of any strong peaks around 600 nm in dark-field spectra of sharp Au tips suggests that any plasmons present are weakly coupled and do not scatter strongly in this illumination geometry. Such plasmons may still couple with the opposing tip to form a gap mode but reduced scattering efficiency results in a lower observed field enhancement. On the other hand, AuNP tips are well suited to high enhancements when illuminated at the appropriate plasmonic resonances. Whilst a number of plasmonic probes have been developed recently, several useful features are obtained here. By using standard AFM probes as a basis, these AuNP tips maintain their functionality as AFM probes for force microscopy. The metallic coating of these tips also allows for simultaneous electrical measurements whilst performing optical and AFM force measurements. These tips therefore function as standard electrical AFM probes with added plasmonic functionality. Furthermore, such tips also show excellent resistance to damage at the tip apex after multiple surface contacts, though surfaces do become deformed after heavy use. Their robust nature is attributed to the direct growth of the AuNP root across the pyramidal tip end. This is a

⁹Note that these widths are below the quantum limit for such large AuNPs, presented in [22], only because the opposing tip has such a small radius to increase localisation.

significant improvement over currently-available commercial spherical AFM tips, in which the spheres break from the tip and adhere to the contact surface after only one or a small number of contact cycles. Further applications of spherical metallic tips can be envisaged, for instance in plasmonic optical trapping [43] because the tips in the present geometry can conveniently act as a heat sink reducing the problematic optical heating observed, and resulting thermal damage.

1.4 Conclusions

Within this chapter it has been shown that spherical AuNP-tipped AFM probes are capable of supporting radiative LSPs in the red part of the visible spectrum that are not supported by the more conventional, sharp Au tips. These plasmons are clearly observed to exist at the apex of extended tip microstructures using scanning confocal hyperspectral imaging in the SDF microscope platform to locally probe the optical response. Broadband tuneable SERS is used to further confirm plasmonic behaviour in spherical Au tips. These techniques are ones that enables plasmon-dependent applications, such as TERS, to pre-screen nanostructured tips to better improve their reliability and reproducibility. The development of antenna-like plasmons in tips through nanostructuring, which readily couple to light without the need for momentum matching, is a step forward for TENOM. Furthermore, these modes determine what plasmonic phenomena are able to be experimentally observed, hence spherical tips can be used to dynamically investigate plasmonics.

References

- [1] R. A. Schultz et al., *Cytometry* **43**, 239–247 (2001).
- [2] S. J. Leavesley et al., *Journal of biophotonics* **5**, 67–84 (2012).
- [3] E. K. Hege et al., in *Optical science and technology, spie's 48th annual meeting* (International Society for Optics and Photonics, 2004), pp. 380–391.
- [4] J. A. Hackwell et al., in *Spie's 1996 international symposium on optical science, engineering, and instrumentation* (International Society for Optics and Photonics, 1996), pp. 102–107.
- [5] G. A. Shaw and H.-h. K. Burke, *Lincoln Laboratory Journal* **14**, 3–28 (2003).
- [6] M. Kim, Y. Chen, P. Mehl, et al., *Transactions-American Society of Agricultural Engineers* **44**, 721–730 (2001).
- [7] A. Gowen et al., *Trends in Food Science & Technology* **18**, 590–598 (2007).
- [8] T. Vo-Dinh, *Engineering in Medicine and Biology Magazine, IEEE* **23**, 40–49 (2004).
- [9] M. E. Martin et al., *Annals of biomedical engineering* **34**, 1061–1068 (2006).
- [10] G. Lu and B. Fei, *Journal of biomedical optics* **19**, 010901–010901 (2014).
- [11] L. Herrmann et al., *Optics express* **21**, 32377–32385 (2013).
- [12] M. Bashevoy et al., *Optics express* **15**, 11313–11320 (2007).
- [13] M. Iga et al., *Review of Scientific Instruments* **83**, 103707 (2012).
- [14] R. W. Slawson, Z. Ninkov, and E. P. Horch, *Publications of the Astronomical Society of the Pacific* **111**, 621–626 (1999).
- [15] N. Gat, in *Aerosense 2000* (International Society for Optics and Photonics, 2000), pp. 50–64.
- [16] J. T. Daly et al., in *Symposium on integrated optoelectronics* (International Society for Optics and Photonics, 2000), pp. 104–115.
- [17] T. Okamoto and I. Yamaguchi, *Optics letters* **16**, 1277–1279 (1991).
- [18] T. V. Bulygin and G. N. Vishnyakov, in *Analytical methods for optical tomography* (International Society for Optics and Photonics, 1992), pp. 315–322.
- [19] T. Okamoto, A. Takahashi, and I. Yamaguchi, *Applied Spectroscopy* **47**, 1198–1202 (1993).
- [20] M. Descour and E. Dereniak, *Applied Optics* **34**, 4817–4826 (1995).
- [21] S. Grusche, *Applied optics* **53**, 4594–4603 (2014).

- [22] K. J. Savage et al., *Nature* **491**, 574–577 (2012).
- [23] A. Sanders et al., *Particle & Particle Systems Characterization* **32**, 182–187 (2015).
- [24] W. Zhang, X. Cui, and O. J. Martin, *Journal of Raman Spectroscopy* **40**, 1338–1342 (2009).
- [25] A. Lombardi and L. Weller, in preparation (2015).
- [26] J. T. Hugall and J. J. Baumberg, *Physical Review Letters* (2015).
- [27] M. I. Stockman, *Optics express* **19**, 22029–22106 (2011).
- [28] C. Huber et al., *Physical Chemistry Chemical Physics* **16**, 2289–2296 (2014).
- [29] J. Mock et al., *The Journal of Chemical Physics* **116**, 6755–6759 (2002).
- [30] H. Kuwata et al., *Applied physics letters* **83**, 4625–4627 (2003).
- [31] B. Ren, G. Picardi, and B. Pettinger, *Review of Scientific Instruments* **75**, 837–841 (2004).
- [32] J. Mertens et al., *Nano letters* **13**, 5033–5038 (2013).
- [33] R. W. Taylor et al., *Scientific reports* **4** (2014).
- [34] S. Mahajan et al., *The Journal of Physical Chemistry C* **114**, 7242–7250 (2009).
- [35] P. V. Dudin, P. R. Unwin, and J. V. Macpherson, *The Journal of Physical Chemistry C* **114**, 13241–13248 (2010).
- [36] F. G. De Abajo and J Aizpurua, *Physical Review B* **56**, 15873 (1997).
- [37] F. G. de Abajo and A Howie, *Physical Review B* **65**, 115418 (2002).
- [38] A. Downes, D. Salter, and A. Elfick, *The Journal of Physical Chemistry B* **110**, 6692–6698 (2006).
- [39] J. T. Hugall, J. J. Baumberg, and S. Mahajan, *The Journal of Physical Chemistry C* **116**, 6184–6190 (2012).
- [40] I. Romero et al., *Optics Express* **14**, 9988–9999 (2006).
- [41] B. Pettinger et al., *Annual review of physical chemistry* **63**, 379–399 (2012).
- [42] T. Umakoshi et al., *Applied Physics Express* **5**, 052001 (2012).
- [43] N. C. Lindquist et al., *Laser & Photonics Reviews* **7**, 453–477 (2013).